Published in final edited form as:
Free Radic Biol Med. 2014 September ; 74: 64–73. doi:10.1016/j.freeradbiomed.2014.06.012.

ARSENIC INDUCES SUSTAINED IMPAIRMENT OF SKELETAL MUSCLE AND MUSCLE PROGENITOR CELL ULTRASTRUCTURE AND BIOENERGETICS

Ambrosio Fabrisia,
Department of Physical Medicine & Rehabilitation, University of Pittsburgh, Pittsburgh, PA 15219 ambrosiof@upmc.edu

Brown Elke,
Department of Physical Medicine & Rehabilitation, University of Pittsburgh, Pittsburgh, PA 15219, brownep@upmc.edu

Stolz Donna,
Department of Cell Biology, University of Pittsburgh, Pittsburgh, PA 15213, dstolz@pitt.edu

Ferrari Ricardo,
Department of Physical Medicine & Rehabilitation, University of Pittsburgh, Pittsburgh, PA, ferrarirj@upmc.edu

Goodpaster Bret,
Department of Medicine, University of Pittsburgh, Pittsburgh, PA 15213, bgood@pitt.edu

Deasy Bridget,
Department of Orthopaedic Surgery, University of Pittsburgh, Pittsburgh, PA 15213, deasybm@gmail.com

Distefano Giovanna,
Department of Physical Therapy, University of Pittsburgh, Pittsburgh, PA, 15213, gid7@pitt.edu

Roperti Alexandra,
Department of Bioengineering, University of Pittsburgh, Pittsburgh, PA, 15213, arr77@pitt.edu

Cheikhi Amin,
Department of Environmental and Occupational Health, University of Pittsburgh, Pittsburgh, PA, 15219, amc165@pitt.edu

Garciafigueroa Yesica, and
Department of Environmental and Occupational Health, University of Pittsburgh, Pittsburgh, PA, 15219, dyg1@pitt.edu

Corresponding Author: Fabrisia Ambrosio, PhD, PT, 450 Technology Drive, Suite 308, Bridgeside Point Building II, Pittsburgh, PA 15219, ambrosiof@upmc.edu, 412-624-5276.

Barchowsky Aaron
Department of Environmental and Occupational Health, University of Pittsburgh, Pittsburgh, PA, 15219, aab20@pitt.edu

Abstract

Over 4 million individuals in the US, and over 140 million individuals worldwide, are exposed daily to arsenic-contaminated drinking water. Human exposures can range from below the current limit of 10 μg/L to over 1 mg/L, with 100 μg/L promoting disease in a large portion of those exposed. Although increased attention has recently been paid to myopathy following arsenic exposure, the pathogenic mechanisms underlying clinical symptoms remain poorly understood. This study tested the hypothesis that arsenic induces lasting muscle mitochondrial dysfunction and impairs metabolism. When compared to non-exposed controls, mice exposed to drinking water containing 100μg/L arsenite for 5 weeks demonstrated impaired muscle function, mitochondrial myopathy, and altered oxygen consumption that were concomitant with increased mitochondrial fusion gene transcription. There was no difference in levels of inorganic arsenic or its mononomethyl- and dimethyl- metabolites between controls and exposed muscles, confirming that arsenic does not accumulate in muscle. Nevertheless, muscle progenitor cells isolated from exposed mice recapitulated the aberrant myofiber phenotype and were more resistant to oxidative stress, generated more reactive oxygen species, and displayed autophagic mitochondrial morphology, as compared to cells isolated from non-exposed mice. These pathological changes from a possible maladaptive oxidative stress response provide insight into declines in muscle functioning caused by exposure to this common environmental contaminant.

Keywords

metabolism; mitochondria; resistance to stress

INTRODUCTION

While the widely reported incidence of arsenic (As(III)) use in past centuries for medicinal, industrial, and homicidal purposes has declined dramatically, modern times have seen resurgence in the attention paid to this organic metalloid. This is due, in large part, to the increasingly recognized presence of As(III) in the food and drinking supplies serving more than 140 million individuals worldwide and nearly 4 million individuals in the United States alone. Unfortunately, the very same characteristic that makes As(III) such an effective tool for acute poisoning also makes it a dangerous environmental contaminant: it is largely undetected because it is odorless, tasteless and colorless. Increasingly, however, As(III) is being recognized for its adverse, yet clandestine, effects on tissue functioning and regenerative capacity, even at low, everyday concentrations.

As(III) is a semi-metal element that seeps into drinking water supplies through natural deposits in the earth. In addition to causing a number of cancer and non-cancer diseases, common symptoms accompanying arsenic exposure include muscle weakness, atrophy, sensorimotor impairment; symptoms that are present in 10–14 million of exposed individuals (1–3). The most complete epidemiologic studies that investigated As(III)-

induced weakness demonstrated that 35–85% of individuals in As(III)-endemic regions presented with weakness and neuropathies (1, 2, 4). Electromyographic analysis of symptoms indicated that 7.5–10% of exposed individuals had sensorimotor deficits, atrophy, and impaired gait (1, 2). Parvez *et al* identified an inverse relationship between As(III) exposure (average water exposure 43 μg/L, producing blood levels of 6.3 μg/L (83 nM)) and motor functioning, strength and agility in 8–11 year-old children (3). These studies were somewhat limited in subject numbers (less than 1000) and to one region of the world. However, they have significant implications for disease prevalence given the large numbers of individuals exposed to greater than 10 μg/L of As(III) in their drinking water. Thus, this very significant environmental exposure may be surreptitiously contributing to atrophy, muscle weakness and disability in a large population. This is important, as muscle weakness is among the greatest factors contributing to declines in functional mobility (reviewed in (5)) and is a strong predictor of mortality (6).

While muscular sequelae following As(III) toxicity are often attributed to secondary neurological effects (7, 8), recent studies indicate direct As(III) actions on muscle composition and muscle stem cells that impair proliferation and myogenic differentiation (9, 10), findings that may help explain the above referenced clinical symptoms. Muscle stem cells directly influence the ability of skeletal muscle to grow or repair in response to a stressor (injury, disease, or exercise), a response that is largely dependent on the microenvironment, or niche. The niche is dynamic and characterized by the presence of autocrine and paracrine factors, as well as extracellular matrix proteins. Chronic As(III) exposure has been associated with modulation of tissue microenvironment as characterized by a modification of matrix components (11), aberrant angiogenesis and vessel remodeling (12, 13), and increased fibrosis (14, 15). *In vivo* (9) and *in vitro* (10) studies demonstrate a dose-dependent As(III) impairment of muscle regeneration, decreased myotube formation from isolated myoblasts and decreased activation of the myogenic molecular program (10).

Mitochondrial myopathy and dysfunction appear to be involved in As(III)-induced pathogenesis in muscle. However, the pathogenic mechanisms of arsenic's action in muscle or muscle progenitor cells that are required for muscle regeneration are unresolved. These studies focus on the impact of low to moderate As(III) exposures commonly encountered in the environment on skeletal muscle tissue and stem cell pathologies. We hypothesized that *in vivo* exposure to As(III) results in a maladaptive myofiber phenotype with dysfunctional mitochondria and altered bioenergetics that contribute to a decreased force producing capacity. Moreover, we hypothesized that muscle progenitor cells are a target of As(III) and display an altered metabolic profile that parallels alterations observed at the myofiber level.

MATERIALS & METHODS

Animal exposure

Five to 6 week old male wild type C57BL/6NTac (Taconic Farms, Hudson NY) mice were exposed for 2–5 weeks to drinking water containing 0 or 100 μg/L trivalent arsenite (As(III)), as previously described (12, 13). All studies were approved by the Institutional Animal Care and Use Committee of the University of Pittsburgh. As(III) was used in these studies as it is the most relevant toxic inorganic arsenic species. Further, these levels are

within the range of exposures in large epidemiological studies of arsenic effects on motor function demonstrating motor deficits in children (29). Fresh As(III)-containing water or culture media is provided every 2–3 days mice or cultured cells to insure that there is little As(III) oxidation to As(V).

Quantification of As(III) within muscle tissue

Muscle tissue from control and five week As(III) exposed mice was flash frozen in liquid nitrogen, shipped on dry ice to Dr Miroslav Styblo at the University of North Carolina for quantiation of As(III) and its metabolites. Arsenic species were analyzed by hydride generation-cryotrapping-ion-coupled plasma mass spectrometry (HG-CT-ICP-MS) using methods previously developed for HG-CT-atomic absorption (30, 31).

In situ contractile testing

Anterior compartment muscle strength of animals exposed to 0 or 100μg/L of arsenic for 5 weeks was evaluated using an *in situ* testing apparatus (Model 809B, Aurora Scientific Inc, Canada). Briefly, the foot was secured onto a footplate in 20° of plantar flexion and the peroneal nerve of anesthetized animals was isolated and stimulated using a needle electrode, as previously described (16). This method allows for determination of muscle contractile properties while maintaining normal muscle orientation, innervation and vascular supply. Initially, muscle peak twitch, time to peak twitch and half-relaxation time were evaluated. Tetanic contractions (350ms train) at 10, 30, 50, 80, 100, 120, 150 Hz were elicited to obtain a force-frequency curve, with a 2-minute rest between each contraction. Results of single stimulations and tetanic contraction were collected in torque (milliNm). From torque measurements, the specific muscle force was obtained by normalizing the absolute force values (milliN) to the calculated muscle crosssectional area (CSA). CSA was calculated as described by Brooks and Faulkner (17). Following assessment of peak force production and recovery (approximately 10 minutes), animals were subjected to a 7-minute high-frequency fatiguing protocol. Every 4 seconds, the muscle was exposed to a 350ms train stimulation at 100Hz, as we previously described (16). Force recovery was analyzed at 5 and 10 min following completion of the fatiguing protocol.

Muscle Precursor Cell Isolation

Following 0 (control) or 5 weeks of exposure, hindlimb muscles from animals (n=3–4/group) were harvested for progenitor cell isolation, using a modified pre-plate technique, as previously described (18–20). Briefly, following hindlimb muscle enzymatic digestion, the homogenate was serially plated (3 times) onto collagen-coated flasks. It has been previously shown that cells that rapidly adhere to the collagen-coated flasks are predominantly of a fibroblastic lineage (19). On the other hand, those late-adhering cells, isolated after 3–4 serial passages, have been previously characterized as having a myogenic lineage (19). All cells were expanded in high serum proliferation media (DMEM, 10% fetal bovine serum, 10% horse serum, 1% penicillin/streptomycin, and 0.5% chick embryo extract). Precursor cells were cultured for <6 passages before each experiment.

Prior to analysis, cells were characterized using flow cytometry, as described by Cheung et al (21). Briefly, isolated cells were co-stained with Vcam-biotin (clone 429; BD Bioscience),

CD31-APC (clone MEC 13.3; BD Bioscience), CD45-APC (clone 30-F11; BD Bioscience) and Sca-1-Pacific-Blue (clone D7; Biolegend) at 1:75. Streptavidin-PE-cy7 (BD Biosciences, 1:75) was used to amplify the Vcam signal. Cell sorting was performed using a BD FACSAria (Becton, Dickenson and Co, San Jose, CA). Expression of paired box transcription factor, Pax 7, was also performed to further confirm purity of the satellite cell population (22).

Live Automated Cell Imaging (LACI)

Once muscle progenitor cells were isolated, they were trypsinized and plated onto 24-well plates at a density of 790 cells/cm2 in high serum media, and allowed to adhere for at least 4 hours. After 4 hours, muscle progenitor cell growth kinetics of isolated from control and arsenic-treated muscle were calculated using Live Automated cell Imaging (LACI). LACI was used to measure cell growth curves and population doubling times across groups, as previously described (23). Images at a 10× objective were taken every 10 minutes for a total of 72 hours, allowing for real-time, nondestructive kinetic analysis of phenotypic changes in living cell populations. The total cell number/ high power field of view was manually quantified at 0, 12, 24, 36, and 60-hour time points, using Image J software (National Institutes of Health, Bethesda, MD). The population doubling time (PDT), calculated as T/(log2[Nf/No]), where T= time in culture, No= initial number of cells, and Nf= final number of cells, was determined. For each group, cells were plated in triplicate and were analyzed by a blinded investigator.

Resistance to Oxidative Stress

Cells from control and 5-week arsenic groups were plated on collagen-coated 24-well plate at the density of 790cells/cm^2 with high serum proliferation media as described above. H_2O_2 was then added to the media (200 μM) to induce oxidative stress. Cell expansion for control and arsenic-derived muscle progenitor cells in the presence of H2O2 were then compared to non-stressed counterparts.

Histology

Following 0 or 5 weeks of As(III) exposure, mice in each group were euthanized with CO2. Hindlimb muscles were removed and snap frozen in nitrogen-cooled 2-methylbutane (Hematoxylin and eosin (H&E). Cryopreserved muscles were sectioned at 10 μm. H&E stains were performed to provide a qualitative representation of the muscle structures following arsenic exposure. Using Image J software, the average myofiber area was determined by manually tracing 200 myofibers/cross-section over 6 sections, for a total of 1200 myofibers per group.

Transmission Electron Microscopy (TEM)

Portions of tibialis anterior skeletal muscle were fixed in 2.5% gluteraldehyde and processed for TEM as previously described (13). Ultrathin (70nm) sections were imaged using a JEM 1011 TEM (JEOL, Peabody, MA) at 80kV. Images were taken using a side-mount AMT 2k digital camera (Advanced Microscopy Techniques, Danvers, MA).

Cells grown on tissue culture plastic ware were fixed in 2.5% gluteraldehyde in 100 mM PBS (8 gm/l NaCl, 0.2 gm/l KCl, 1.15 gm/l Na2HPO4.7H2O, 0.2 gm/l KH2PO4, pH 7.4) overnight at 4°C. Monolayers were then washed in PBS three times then post-fixed in aqueous 1% osmium tetroxide, 1% Fe6CN3 for 1 hr. Cells were washed 3 times in PBS then dehydrated through a 30–100% ethanol series then several changes of Polybed 812 embedding resin (Polysciences, Warrington, PA). Cultures were embedded in by inverting Polybed 812-filled BEEM capsules on top of the cells. Blocks were cured overnight at 37°C, and then cured for two days at 65°C. Monolayers were pulled off the coverslips and re-embedded for cross section. Ultrathin cross sections (60 nm) of the cells were obtained on a Riechart Ultracut E microtome, post-stained in 4% uranyl acetate for 10 min and 1% lead citrate for 7 min.

High-resolution respirometry

Mitochondrial respiration of freshly isolated, permebealized myofibers was evaluated using high-resolution respirometry Oxygraphy-2k (Oroboros® Instruments, Innsbruck, Austria) and Oroboros DataLab software for data acquisition and analysis (as described (24, 25)). Briefly, muscles harvested from control or As(III)-exposed mice were manually teased apart into loosely bound fiber bundles, permeabilized with saponin, washed and placed in respirometry chambers. Assays are performed at 37°C in the range of 230-150 μM oxygen and start with flux stabilization of the fiber bundle without substrates. Respiration was tested with addition of pyruvate, malate, and glutamate. Maximal coupled or state 3 respiration was then measured following sequential addition of: ADP; cytochrome c to check the quality of the muscle fiber preparation and the intactness of the outer mitochondrial membrane; and finally succinate (complex I and complex II respiration). Leak respiration (proton and electron slip with proton leak) in intact, non-permeabilized cells was measured in the presence oligomycin that prevents ATP synthesis. Maximal uncoupled rate was determined by adding the uncoupling agent carbonylcyanide-p-trifluoromethoxyphenylhydrazone (FCCP). Rotenone was then added to inhibit complex Ito measure maximum transport capacity with complex II substrates only. Finally, mitochondrial oxygen consumption was inhibited with antimycin A (5μM) to confirm the predominance of the mitochondrial electron transport chain of total oxygen consumption. Following the respirometry assay, fiber bundles were recovered and air-dried. The dry weight of the fiber bundle was then measured and steady state O_2 flux for each respiratory state and normalized to fiber bundle dry weight using Datlab 4 software (Oroboros Inc., Innsbruck, Aus). Results are presented as pmol O2/sec*mg DW. Data obtained from cells were normalized to cell number.

MitoSox analysis

Cells were seeded on 35mm glass bottom dishes (MatTek Corporation, Ashland, MA) and incubated with 5 μM MitoSOX™ Red and MitoTracker® Green FM (Invitrogen, Eugene, OR) for 15 minutes at 37 °C. Cells were washed with PBS, the media replaced and the dish inserted in a closed, thermo-controlled (37°C) stage top incubator (Tokai Hit Co., Shizuoka-ken, Japan) atop the motorized stage of an inverted Nikon TiE fluorescent microscope (Nikon Inc., Melville, NY) equipped with a 60X oil immersion optic (Nikon, CFI PlanFluor, NA 1.4) and NIS Elements Software. MitoSOX™ Red MitoTracker® Green was excited

using a Lumencor diode-pumped light engine (SpectraX, Lumencor Inc., Beaverton OR) and detected using DsRed and EGFP longpass filter sets (Chroma Technology Corp) and a Photometrics CoolSNAP HQ2 camera (Photometrics, Tucson, AZ). Data was collected in 8–12 cells per stage position, with 10 stage positions for each condition. Images were thresholded based on the MitoTracker® Green emissions, and the emission intensity of the MitoSOX™ Red signal within the thresholded region (mitochondrial area) was quantified for each stage position using NIS Elements.

Muscle gene transcripts

RNA was extracted with Trizol (Invitrogen) from the hindlimb muscle of animals exposed to 0 or 100ppb As(III) drinking water for 5 weeks (n=8 each group), and analyzed for transcript levels by quantitative RT-PCR, essentially as described (26). Gene transcripts were quantified using standard curves for the respective cDNA products and changes in resulting inducible cDNA levels were normalized to changes in the housekeeping transcript Rpl41 levels to calculate the pg of normalized product per ml of reaction. Specific primer pairs include mitofusin2 (forward:5'TGATAAGTTTTGCCTGGATGC3': reverse: 5'GGAAGAACTGCTTCTCCGTCT3'), Opa1 (forward:5' AAGATCTAAGGGTTGCGGTGT3': reverse:5' AAGATCTAAGGGTTGCGGTGT3'), Oma1 (forward:5' GAGTGAATAACCTGGCCAACA 3': reverse:5' CATTTACTGCTCGGAGCTTTG3'), and Rpl41 (forward: 5'AAGATGAGGCAGAGGTCCAA3': reverse:5'GGTTGTAAGAAAGGCGGTCA3').

Statistical analyses

Data are expressed, as means ± SEM. Significance between groups was determined by student's t-tests or, in the case of cellular growth and muscle fatigue/recovery kinetics, a two-way ANOVA. Slopes of muscle fatigue were compared for significant difference by linear regression analysis. A priori, differences were considered to be significantly different at $p<0.05$. Statistical analysis was performed using Graphpad Prizm v5 software.

RESULTS

General health effects of arsenic exposure

Consistent with our previous reports (12, 27), there were no obvious health differences between the control mice and mice that drank water containing 100 μg/L arsenic for 5 weeks. This exposure does not change animal weights and liver/body weight ratio (12, 27), suggesting that food and water intake was equal between the groups. As we found in liver (27), there was also no difference in muscle tissue levels of inorganic arsenic or its major mononomethyl- and dimethyl- metabolites between control and exposed mice (Table I). These data confirm earlier reports that arsenic does not accumulate in mouse tissues until drinking water levels exceed 1.0 ppm. The lack of arsenic accumulation in muscle suggests that little or no As(III) or metabolites remain in the progenitor cells cultured from the As(III)-exposed mice.

Arsenic effects on muscle function, structure and bioenergetics

Exposure to 100 μg/L As(III) for 5 wk caused a number of pathologic changes in the mouse skeletal muscle. Physiological tests of muscle function demonstrated that As(III) trended towards increased peak tetanic torque production and required higher frequency stimulation to produce a maximal tetanic force (Table II). In addition, the muscles of arsenic-exposed mice had decreased resistance to fatigue and decreased force recovery after a fatiguing protocol (Fig 1). We previously reported that As(III) caused mild disruption of the muscle fibers and increased ectopic perivascular lipid accumulation (28). The images and data in Fig 2 show that arsenic increased the average myofiber area, relative to unexposed control fibers. Ultrastructural analysis (TEM) of intact tibialis muscle tissue (Fig 3A) revealed that As(III) exposure disrupted normal mitochondrial morphology. The mitochondria from As(III)-exposed mice had a “swollen” appearance with disrupted cristae and vacuoles, suggestive of impaired mitochondrial fusion and mytophagy. Dysfunctional mitochondrial fusion was supported by increased transcript expression of the fusion proteins mitofusin2 and Opa1, relative to control muscle, as well as in increase in the metalloprotease Oma1 (Table III). Comparison of mitochondrial bioenergetics in muscle fibers isolated from control and exposed mice demonstrated that As(III)-exposed fibers had increased oxygen consumption and mitochondrial activity with possible uncoupling at all complexes in the respiratory chain (Fig 3B).

Sustained effects of As(III) on muscle progenitor cell bioenergetics and function

To investigate the impact of As(III) on regenerative capacity of the muscle, muscle progenitor cells were isolated from animals exposed to 0 or 100 μg/L As(III) for 2 or 5 weeks. Isolated cells were confirmed to be 90.9% (As(III)) and 90.5% (Control) Vcam+/CD31−CD45−/Sca1−, indicative of proliferating myogenic precursor cells (21). Moreover, 96.2% and 92.6% of cells were positive for Pax7 in populations isolated from control and As(III)-exposed animals, respectively (see supplemental Fig 1).

Live Automated Cell Imaging suggested that there was no effect of As(III) on the *in vitro* growth kinetics of the isolated progenitor cells, as indicated by the absence of statistically significant differences between cellular division times for muscle progenitor cells after 5 weeks of arsenic exposure and cells from non-treated controls (Controls: 22+/−6 hrs; 5 week: 19+/−6 hrs; p=0.288).

Consistent with observations in whole muscle, TEM images of progenitor cells isolated from the muscles of mice exposed to As(III) for 2–5 weeks to arsenic retained “swollen” and amorphic mitochondria relative to mitochondria in muscle progenitor cells isolated from control mice (Fig 4A). In addition, progenitor cells isolated from mice exposed to As(III) for 5 weeks had sustained increases in numbers and size of lysosomes and autophagolysosomes (Fig 4A), suggesting that they retain an autophagic phenotype in the absence of arsenic. Also consistent with the *in vivo* effects in muscle, analysis of the progenitor cell bioenergetics revealed that cells isolated from 5 week As(III)-exposed mice had increased mitochondrial oxygen consumption. When oligomycin was added to inhibit oxidative phosphorylation and measure LEAK respiration (24), the muscle progenitor cells from

As(III)-exposed mice had a 2-fold increase in proton leak relative control cells (Fig 4B). This indicated increased uncoupling of respiration.

As(III)-induced muscle progenitor cell phenotype retains increased oxidant production and resistance to stress

The mitochondrial LEAK respiration in the presence of oligomycin is composed of proton leak and slip, as well as electron slip that diverts electrons to ROS generation (24). Live cell imaging of Mitosox oxidation was used to compare this ROS generation in muscle progenitor cells isolated from control and As(III)-exposed mice. Mitosox is predominantly oxidized by mitochondrial superoxide, and that data in Fig 5 indicate that the mitochondria from exposed mice retain a significantly elevated level of superoxide production. After demonstrating that the muscle progenitor cells from the As(III)-exposed mice had a marked increase in ROS, we investigated how this impacted their sensitivity to oxidative stress. When challenged with a high concentration of H_2O_2, the number of muscle progenitor cells from control mice decreased over the 72 h observation period (Fig 6). In contrast, the number of cells isolated from mice exposed for 5 wk to As(III) were static for 48 h after the addition of H_2O_2, after which time cell numbers began to increase (Fig 6). This finding suggests that the cells from As(III)-exposed mice retained a phenotype that both generated increased ROS and was highly resistant to oxidative stress.

DISCUSSION

The data presented support the hypothesis that skeletal muscle mitochondria and progenitor cells are targeted by arsenic and that *in vivo* exposure produces a maladaptive progenitor cell phenotype with dysfunctional mitochondria, excess oxidant production, and resistance to oxidative stress. *In vivo* exposure to an environmentally relevant, moderate level of As(III) in drinking water (unfortunately encountered by millions of individuals worldwide), resulted in a mitochondrial myopathy and altered myofiber bioenergetics. These effects appeared to be recapitulated in isolated muscle progenitor cells, as determined by increased cellular proliferation in the presence of oxidative stress and altered mitochondrial morphology and function.

The observed increase in myofiber area, or hypertrophy, was associated with a significantly increased peak tetanic force production in muscles exposed to As(III). However, As(III)-exposed mice fatigued faster and took longer to recover from fatigue than in control mice. These findings are consistent with a fiber type conversion towards a fast-twitch phenotype. Whereas slow twitch (type I) myofibers are smaller in diameter, display low peak forces and high resistance to fatigue, fast-twitch (type II) myofibers have larger diameters, high peak forces and low resistance to fatigue. The latter results from the decreased mitochondrial metabolic capacity of fast-twitch myofibers that rely on glycolytic activity for energy production. This is opposed to the predominantly oxidative metabolism typical of slow-twitch myofibers that are generally rich in functional mitochondria. It is important to note that whole body and muscle metabolic economy are negatively related to type II myofiber area (29).

Indeed, the decreased muscle functional capacity and impaired recovery was supported by the multiple pathological ultrastructural changes in the As(III)-exposed muscle and mitochondria. The most striking changes were sarcoplasmic and mitochondrial swelling, as well as disrupted sarcomere organization (Fig 3). The mitochondrial and nuclear swelling with loss of christae and chromatin condensation respectively, as well as disrupted endoplasmic reticulum, are similar to ultrastructural changes observed in cardiac muscle in a mouse model of toxicity from high dose arsenic trioxide (ATO) therapies (30). The pathologic structures were also consistent with the symptoms of muscle morbidity in a patient receiving ATO therapy who presented with profound mitochondrial myopathy and lipid droplet accumulation in skeletal muscle that persisted for months after therapy was stopped (31). The skeletal muscle mitochondrial damage and dysfunction observed in this patient were accompanied by profound muscle weakness that resulted in an inability to walk independently. Importantly, in the current murine study, the ultrastructural changes become progressively more severe over the five weeks of exposure. This was also reflected in the worsening mitochondrial morphology and increased mitophagy observed in muscle progenitor cells that was retained in culture and in the absence of continued As(III) exposure (Fig 3). The pathologic implications of these observations are that exposure to even moderate levels of As(III) may target mitochondrial bioenergetics in the myofibers to reduce the amount of energy available for muscle maintenance and force production. These alterations may explain the frequent reports of muscle weakness and disability following chronic arsenic exposure (1–3).

The increased mitochondrial oxygen consumption by muscle progenitor cells isolated from exposed mice was maladaptive and associated with increased ROS levels when compared to cells isolated from non-exposed control mice (Fig 3 and 4). Given the similar oxygen consumption profile seen in As(III)-exposed myofibers (Fig 2), it is likely that there was also elevated ROS generation by the dysfunctional myofiber mitochondria *in vivo*. Previous studies demonstrated that C2C12 myoblasts cultured in the presence of ATO increases intracellular ROS levels within hours of the stimulus (9). It was suggested that As(III) stimulates the production of ROS through changes in the mitochondrial membrane integrity and mitochondrial biogenesis (32, 33), which would be consistent with the observed As(III)-induced changes in muscle and muscle progenitor cell mitochondrial morphology (Figs 2,3). Other sources of ROS, such as As(III)-stimulated NADPH oxidase, cannot be ruled out, however, as these have been shown to be essential for As(III)-induced endothelial dysfunction and vascular remodeling (13, 34). While it is well-known that mitochondria are direct targets of As(III) and that chronic As(III) exposure elevates mitochondrial ROS (32, 33), the novel observation that increased muscle progenitor cell oxygen consumption and associated ROS production is sustained even after removal of the of As(III) stimulus suggests that epigenetic regulation of cell phenotype may be critical in generating maladaptive, dysfunctional myofibers and progenitor cells. It may be that the As(III)-induced ROS accumulation creates dysfunctional mitochondria, rather than exerting a direct action on respiration (35). Alternatively, the increased ROS generation may be a part of a feed-forward cycle of dysfunctional homeostasis.

As(III)-induced dysfunctional myofiber and muscle progenitor cell phenotypes with "swollen" and "degenerating" mitochondria, autophagic mitochondria, and autophagolysosomes may result from a maladaptive response to the As(III)-induced oxidants. This was suggested for cultured airway epithelial cells following long term culture with As(III) (32). Indeed, sub-lethal stress induces protection of myocytes and myoblasts from high-level H_2O_2, which, in turn, induces mitochondrial death and apoptosis (36). It is clear from the data in Fig 6 that excess H_2O_2 reduces the number of muscle progenitor cells isolated from control mice. However, despite exposure to this high level of oxidative stress, progenitor cells isolated from animals exposed to As(III) were resistant to oxidant injury and displayed increased cellular proliferation several days after removal of the oxidant stimulus. Proliferation in response to stress increases the cellular demand for energy, a demand that is met by the function of mitochondria. The *in vivo* As(III) exposure generated a phenotype with mitochondria that undergo autophagy rather than current leak that promotes apoptosis. It is interesting that the duration of *in vivo* exposure resulted in different degrees of protective phenotypic change (Fig 3), in that there was a lower level of mitochondrial change and little increase in lysosomes or autophagolysosomes in cells isolated from mice exposed to As(III) for 2 wk, relative to cells isolated from mice exposed for 5 wk. Mitochondrial damage is a well-established initiation signal for the particular form of autophagy we observed in the cultured cells and the increased turnover of mitochondria following chronic As(III) exposure is a consistent finding in multiple cell types (32, 37). However, it is evident that this is a maladaptive response, as it may lead to pathogenic hyperproliferation and dysfunction in response to stress (32, 37).

Environmental exposures may induce changes in precursor cell responses and function, thereby initiating a devastating cascade of compromised tissue structure and function. Experiments examining skeletal muscle regeneration following an acute injury in mice exposed acutely to 10 to 100 times more As(III) than in the current study demonstrated that As(III) delays healing, as evidenced by a decreased number of actively regenerating myofibers and increased fibrosis (9). The decreased regenerative response was consistent with decreased myogenicity and expression of myogenesis-associated genes in the immortalized C2C12 myoblasts or in primary mouse myoblasts exposed to As(III) in cell culture (9, 10). While these findings from *in vitro* exposures are consistent with our findings in muscle progenitor cells isolated from As(III)-exposed mice, a major difference with our observations is that moderate levels of *in vivo* exposure progressively impairs muscle progenitor cell function. Since there is no As(III) added to the cultures as the cells go through multiple population doublings, the sustained altered bioenergetics may be caused by As(III)-induced epigenetic repression that does not revert once As(III) has been removed. This epigenetic repression has been suggested by studies demonstrating increased repressive DNA and histone hypermethylation in and near the myogenin and Igf-1 promoters in C2C12 cells following acute *in vitro* As(III) exposures (10, 38). These increased methylations and decreased histone acetylation were associated with increased expression and recruitment of the histone methyltransferase EzH2, as well as recruitment of the DNA methyltransferase, DNMT3a, to the myogenin promoter (38). More extensive studies are needed to determine whether these arsenic-epigenetic marks are responsible for the sustained impairment of progenitors isolated from As(III)-exposed mice and to determine the breadth of epigenetic

change that produces the muscle progenitor cell phenotype with impaired regenerative capacity and dysfunctional bioenergetics.

CONCLUSIONS

Millions of people throughout the United States and worldwide are chronically being exposed to arsenic through food and drinking supplies. Although muscle weakness and declines in functional mobility are often cited as the most common sequelae following high levels of arsenic toxicity, the underlying mechanisms contributing to these clinical symptoms are unknown, as is the biological effect of low to moderate exposures on skeletal muscle structure and function.

Muscle injury and wasting following As(III) exposure are often thought to be secondary to neuropathies (2, 7, 39). However, these and other recent studies indicate direct actions of As(III) on muscle progenitor cell functioning and skeletal muscle homeostasis (9, 10, 38). The *in vivo* effects of As(III) are evident with low to moderate exposure in drinking water, and result in an *in vivo* imprinting of a maladaptive and dysfunctional muscle progenitor cell phenotype. These pathological changes from a maladaptive oxidative stress response have major implications for diminished muscle maintenance, force production and regenerative potential caused by this common environmental exposure. An improved understanding of how such exposures contributes to the complexity of skeletal muscle health is an important first step towards developing targeted and specific interventions aimed at preventing or delaying skeletal muscle declines and, ultimately, health and quality of life for arsenic-exposed individuals.

Supplementary Material

Refer to Web version on PubMed Central for supplementary material.

Acknowledgments

This work was supported by the Pennsylvania Department of Health/ Health Research Program (4100061184), the NIH NIA grant K01AG039477 (FA), the Pittsburgh Claude D. Pepper Older Americans Independence Center (P30 AG024827), NIEHS grant R01ES013781 (AB) and NIEHS grant R01ES023696 (FA & AB).

REFERENCES

1. Chakraborti D, Mukherjee SC, Pati S, Sengupta MK, Rahman MM, Chowdhury UK, Lodh D, Chanda CR, Chakraborti AK, Basu GK. Arsenic groundwater contamination in Middle Ganga Plain, Bihar, India: a future danger? Environ Health Perspect. 2003; 111:1194–1201. [PubMed: 12842773]
2. Mukherjee SC, Rahman MM, Chowdhury UK, Sengupta MK, Lodh D, Chanda CR, Saha KC, Chakraborti D. Neuropathy in arsenic toxicity from groundwater arsenic contamination in West Bengal, India. J Environ Sci Health A Tox Hazard Subst Environ Eng. 2003; 38:165–183. [PubMed: 12635825]
3. Parvez F, Wasserman GA, Factor-Litvak P, Liu X, Slavkovich V, Siddique AB, Sultana R, Sultana R, Islam T, Levy D, et al. Arsenic exposure and motor function among children in Bangladesh. Environ Health Perspect. 2011; 119:1665–1670. [PubMed: 21742576]

4. Guha Mazumder DN. Chronic arsenic toxicity: clinical features, epidemiology, and treatment: experience in West Bengal. J.Environ.Sci Health Part A Tox.Hazard.Subst.Environ.Eng. 2003; 38:141–163.
5. Doherty TJ. Invited review: Aging and sarcopenia. J Appl Physiol. 2003; 95:1717–1727. [PubMed: 12970377]
6. Rantanen T, Harris T, Leveille SG, Visser M, Foley D, Masaki K, Guralnik JM. Muscle strength and body mass index as long-term predictors of mortality in initially healthy men. J Gerontol A Biol Sci Med Sci. 2000; 55:M168–M173. [PubMed: 10795731]
7. Bardullas U, Limon-Pacheco JH, Giordano M, Carrizales L, Mendoza-Trejo MS, Rodriguez VM. Chronic low-level arsenic exposure causes gender-specific alterations in locomotor activity, dopaminergic systems, and thioredoxin expression in mice. Toxicol.Appl.Pharmacol. 2009; 239:169–177. [PubMed: 19121333]
8. Mukherjee SC, Saha KC, Pati S, Dutta RN, Rahman MM, Sengupta MK, Ahamed S, Lodh D, Das B, Hossain MA, et al. Murshidabad--one of the nine groundwater arsenic-affected districts of West Bengal, India. Part II: dermatological, neurological, and obstetric findings. Clin.Toxicol.(Phila). 2005; 43:835–848. [PubMed: 16440511]
9. Yen YP, Tsai KS, Chen YW, Huang CF, Yang RS, Liu SH. Arsenic inhibits myogenic differentiation and muscle regeneration. Environ Health Perspect. 2010; 118:949–956. [PubMed: 20299303]
10. Steffens AA, Hong GM, Bain LJ. Sodium arsenite delays the differentiation of C2C12 mouse myoblast cells and alters methylation patterns on the transcription factor myogenin. Toxicol Appl Pharmacol. 2011; 250:154–161. [PubMed: 20965206]
11. Hays AM, Lantz RC, Rodgers LS, Sollome JJ, Vaillancourt RR, Andrew AS, Hamilton JW, Camenisch TD. Arsenic-induced decreases in the vascular matrix. Toxicol Pathol. 2008; 36:805–817. [PubMed: 18812580]
12. Soucy NV, Mayka D, Klei LR, Nemec AA, Bauer JA, Barchowsky A. Neovascularization and angiogenic gene expression following chronic arsenic exposure in mice. Cardiovasc Toxicol. 2005; 5:29–41. [PubMed: 15738583]
13. Straub AC, Clark KA, Ross MA, Chandra AG, Li S, Gao X, Pagano PJ, Stolz DB, Barchowsky A. Arsenic-stimulated liver sinusoidal capillarization in mice requires NADPH oxidase-generated superoxide. J Clin Invest. 2008; 118:3980–3989. [PubMed: 19033667]
14. Lencinas A, Broka DM, Konieczka JH, Klewer SE, Antin PB, Camenisch TD, Runyan RB. Arsenic exposure perturbs epithelial-mesenchymal cell transition and gene expression in a collagen gel assay. Toxicol Sci. 116:273–285. [PubMed: 20308225]
15. Lantz RC, Chau B, Sarihan P, Witten ML, Pivniouk VI, Chen GJ. In utero and postnatal exposure to arsenic alters pulmonary structure and function. Toxicol Appl Pharmacol. 2009; 235:105–113. [PubMed: 19095001]
16. Distefano G, Ferrari RJ, Weiss C, Deasy BM, Boninger ML, Fitzgerald GK, Huard J, Ambrosio F. Neuromuscular electrical stimulation as a method to maximize the beneficial effects of muscle stem cells transplanted into dystrophic skeletal muscle. PLoS One. 2013; 8:e54922. [PubMed: 23526927]
17. Brooks SV, Faulkner JA. Contractile properties of skeletal muscles from young, adult and aged mice. J Physiol. 1988; 404:71–82. [PubMed: 3253447]
18. Rando TA, Blau HM. Primary mouse myoblast purification, characterization, and transplantation for cell-mediated gene therapy. J Cell Biol. 1994; 125:1275–1287. [PubMed: 8207057]
19. Qu-Petersen Z, Deasy B, Jankowski R, Ikezawa M, Cummins J, Pruchnic R, Mytinger J, Cao B, Gates C, Wernig A, et al. Identification of a novel population of muscle stem cells in mice: potential for muscle regeneration. J.Cell Biol. 2002; 157:851–864. [PubMed: 12021255]
20. Gharaibeh B, Lu A, Tebbets J, Zheng B, Feduska J, Crisan M, Peault B, Cummins J, Huard J. Isolation of a slowly adhering cell fraction containing stem cells from murine skeletal muscle by the preplate technique. Nat.Protoc. 2008; 3:1501–1509. [PubMed: 18772878]
21. Cheung TH, Quach NL, Charville GW, Liu L, Park L, Edalati A, Yoo B, Hoang P, Rando TA. Maintenance of muscle stem-cell quiescence by microRNA-489. Nature. 2012; 482:524–528. [PubMed: 22358842]

22. Seale P, Sabourin LA, Girgis-Gabardo A, Mansouri A, Gruss P, Rudnicki MA. Pax7 is required for the specification of myogenic satellite cells. Cell. 2000; 102:777–786. [PubMed: 11030621]
23. Ambrosio F, Ferrari RJ, Distefano G, Plassmeyer JM, Carvell GE, Deasy BM, Boninger ML, Fitzgerald GK, Huard J. The synergistic effect of treadmill running on stem-cell transplantation to heal injured skeletal muscle. Tissue Eng Part A. 2010; 16:839–849. [PubMed: 19788347]
24. Pesta D, Gnaiger E. High-resolution respirometry: OXPHOS protocols for human cells and permeabilized fibers from small biopsies of human muscle. Methods Mol Biol. 2012; 810:25–58. [PubMed: 22057559]
25. Coen PM, Jubrias SA, Distefano G, Amati F, Mackey DC, Glynn NW, Manini TM, Wohlgemuth SE, Leeuwenburgh C, Cummings SR, et al. Skeletal Muscle Mitochondrial Energetics Are Associated With Maximal Aerobic Capacity and Walking Speed in Older Adults. J Gerontol A Biol Sci Med Sci. 2012
26. Klei LR, Garciafigueroa DY, Barchowsky A. Arsenic activates endothelin-1 Gi protein-coupled receptor signaling to inhibit stem cell differentiation in adipogenesis. Toxicol Sci. 2013; 131:512–520. [PubMed: 23152186]
27. Straub AC, Stolz DB, Ross MA, Hernandez-Zavala A, Soucy NV, Klei LR, Barchowsky A. Arsenic stimulates sinusoidal endothelial cell capillarization and vessel remodeling in mouse liver. Hepatology. 2007; 45:205–212. [PubMed: 17187425]
28. Garciafigueroa DY, Klei LR, Ambrosio F, Barchowsky A. Arsenic-stimulated lipolysis and adipose remodeling is mediated by g-protein-coupled receptors. Toxicol Sci. 2013; 134:335–344. [PubMed: 23650128]
29. Hunter GR, Newcomer BR, Larson-Meyer DE, Bamman MM, Weinsier RL. Muscle metabolic economy is inversely related to exercise intensity and type II myofiber distribution. Muscle Nerve. 2001; 24:654–661. [PubMed: 11317275]
30. Li Y, Sun X, Wang L, Zhou Z, Kang YJ. Myocardial toxicity of arsenic trioxide in a mouse model. Cardiovasc Toxicol. 2002; 2:63–73. [PubMed: 12189281]
31. Echaniz-Laguna A, Benoilid A, Vinzio S, Fornecker LM, Lannes B, Goulle JP, Broly F, Mousson de Camaret B. Mitochondrial myopathy caused by arsenic trioxide therapy. Blood. 119:4272–4274. [PubMed: 22427206]
32. Zhang T, Qi Y, Liao M, Xu M, Bower KA, Frank JA, Shen HM, Luo J, Shi X, Chen G. Autophagy is a cell self-protective mechanism against arsenic-induced cell transformation. Toxicol Sci. 2012; 130:298–308. [PubMed: 22869613]
33. Woo SH, Park IC, Park MJ, Lee HC, Lee SJ, Chun YJ, Lee SH, Hong SI, Rhee CH. Arsenic trioxide induces apoptosis through a reactive oxygen species-dependent pathway and loss of mitochondrial membrane potential in HeLa cells. Int J Oncol. 2002; 21:57–63. [PubMed: 12063550]
34. Smith KR, Klei LR, Barchowsky A. Arsenite stimulates plasma membrane NADPH oxidase in vascular endothelial cells. Am J Physiol Lung Cell Mol Physiol. 2001; 280:L442–L449. [PubMed: 11159027]
35. Samikkannu T, Chen CH, Yih LH, Wang AS, Lin SY, Chen TC, Jan KY. Reactive oxygen species are involved in arsenic trioxide inhibition of pyruvate dehydrogenase activity. Chem Res Toxicol. 2003; 16:409–414. [PubMed: 12641442]
36. Jiang B, Xiao W, Shi Y, Liu M, Xiao X. Heat shock pretreatment inhibited the release of Smac/DIABLO from mitochondria and apoptosis induced by hydrogen peroxide in cardiomyocytes and C2C12 myogenic cells. Cell Stress Chaperones. 2005; 10:252–262. [PubMed: 16184770]
37. Lee CH, Wu SB, Hong CH, Liao WT, Wu CY, Chen GS, Wei YH, Yu HS. Aberrant Cell Proliferation by Enhanced Mitochondrial Biogenesis via mtTFA in Arsenical Skin Cancers. Am.J.Pathol. 2011; 178:2066–2076. [PubMed: 21514422]
38. Hong GM, Bain LJ. Sodium arsenite represses the expression of myogenin in C2C12 mouse myoblast cells through histone modifications and altered expression of Ezh2, Glp, and Igf-1. Toxicol Appl Pharmacol. 2012; 260:250–259. [PubMed: 22426358]
39. Parvez F, Wasserman GA, Factor-Litvak P, Liu X, Slavkovich V, Siddique AB, Sultana R, Sultana R, Islam T, Levy D, et al. Arsenic Exposure and Motor Function among Children in Bangladesh. Environ Health Perspect. 2011; 119

Highlights

- Mitochondrial damage and dysfunction underlie arsenic-induced muscle pathogenesis.
- Muscle and muscle progenitor cell bioenergetics are impaired by arsenic.
- Arsenic-impaired mitochondrial function causes a maladaptive response to oxidants.
- The maladaptive response decreased force producing capacity and fatigue recovery.
- The maladaptive bioenergetics could explain arsenic-promoted muscle disease.

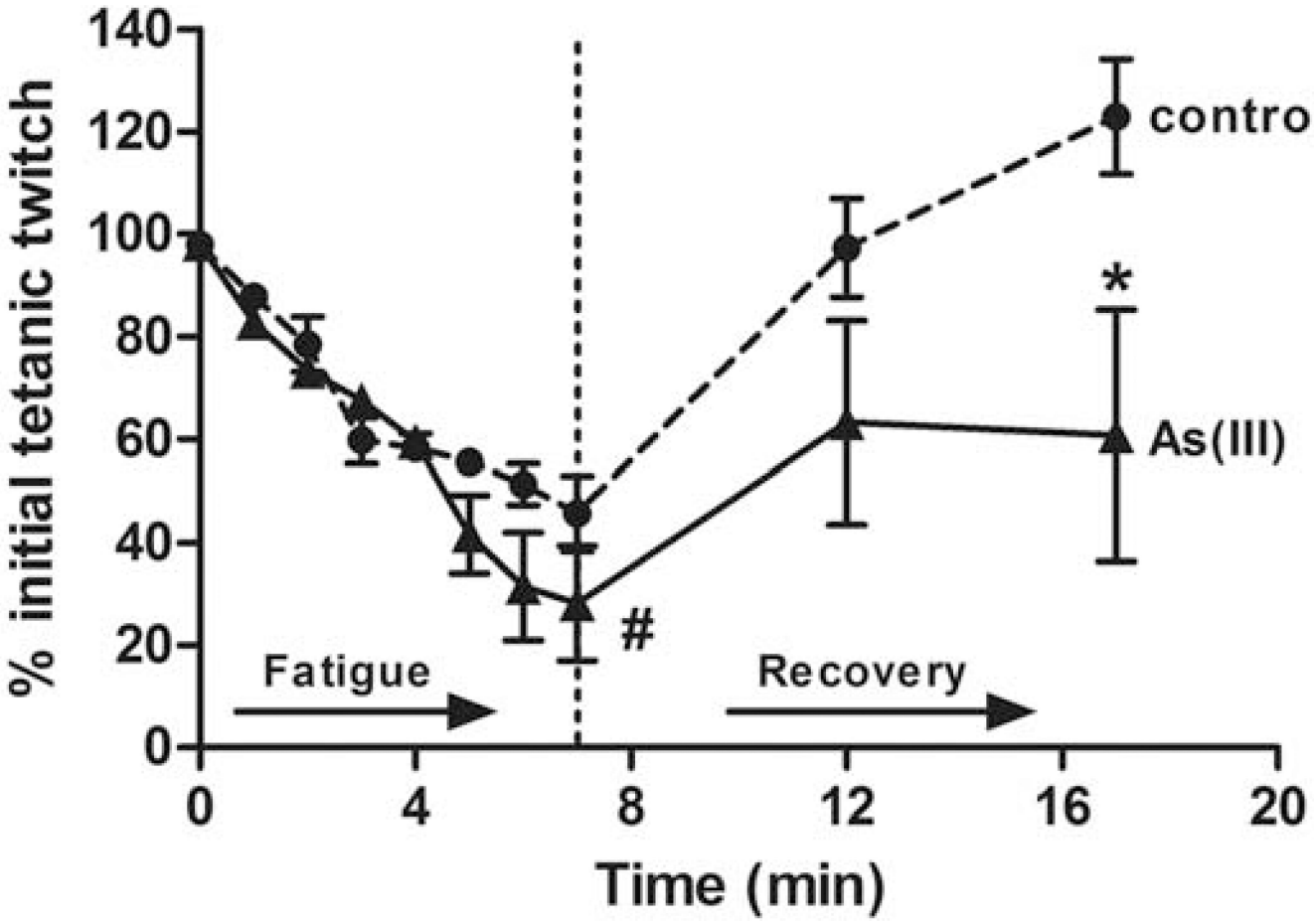

Figure 1.

Arsenic impairs muscle function. Mice were exposed to 0 (n=6) or 100 μg/L (n=5) As(III) in drinking water for 5 wk. At the end of the exposure, muscle contractile function was tested *in situ*, as described in methods. Following assessment of peak force production (Table II), animals were subjected to a 7-minute high-frequency fatiguing protocol with 350ms train stimulation at 100Hz every 4 seconds. Force recovery was analyzed at 5 min following completion of the fatiguing protocol. Data are presented as mean + SEM of the % of starting force. Linear regression analysis demonstrated that the slopes of the control and As(III) fatigue curves are significantly different (#; $p=0.02$). * designates statistical difference from control at $p<0.001$, as determined by two-way analysis of variance.

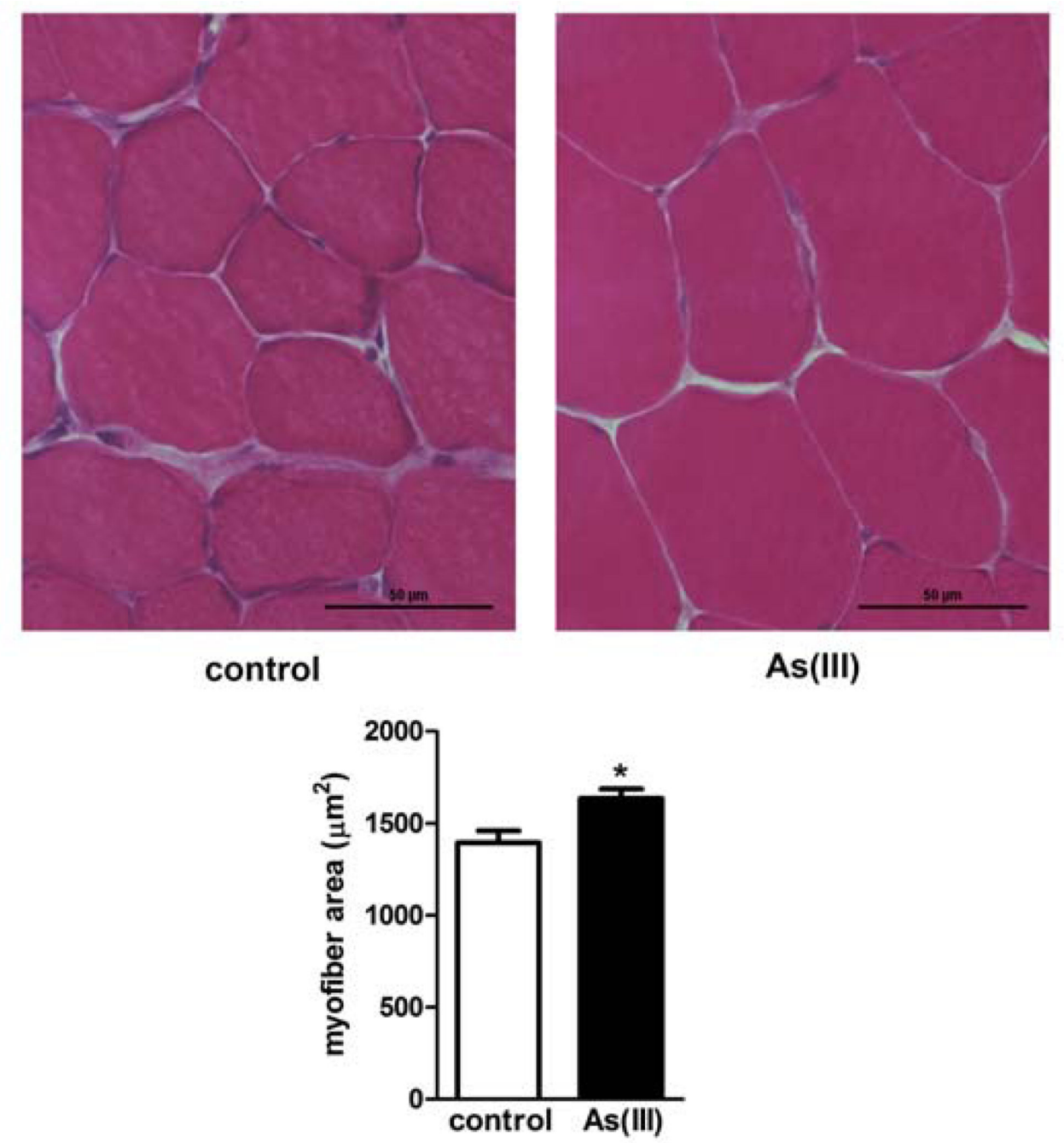

Figure 2.

Arsenic exposure results in myofiber hypertrophy. Mice were exposed to 0 or 100 ppb As(III) in drinking water for 5 wk. At the end of exposure, anterior tibialis muscles were isolated, sectioned and stained with H&E. **A**. shows brightfield 20× images of muscle with increased swollen fibers in the As(III)-exposed mice. **B**. Myofiber area in 50 fibers in each of three cross-sections was quantified and averaged for each mouse and data are presented as mean ± SEM myofiber area in the different exposure groups (As(III) n=6) versus n=7

control muscles). * designates statistical difference from control at $p<0.05$, as determined by a standard t-test.

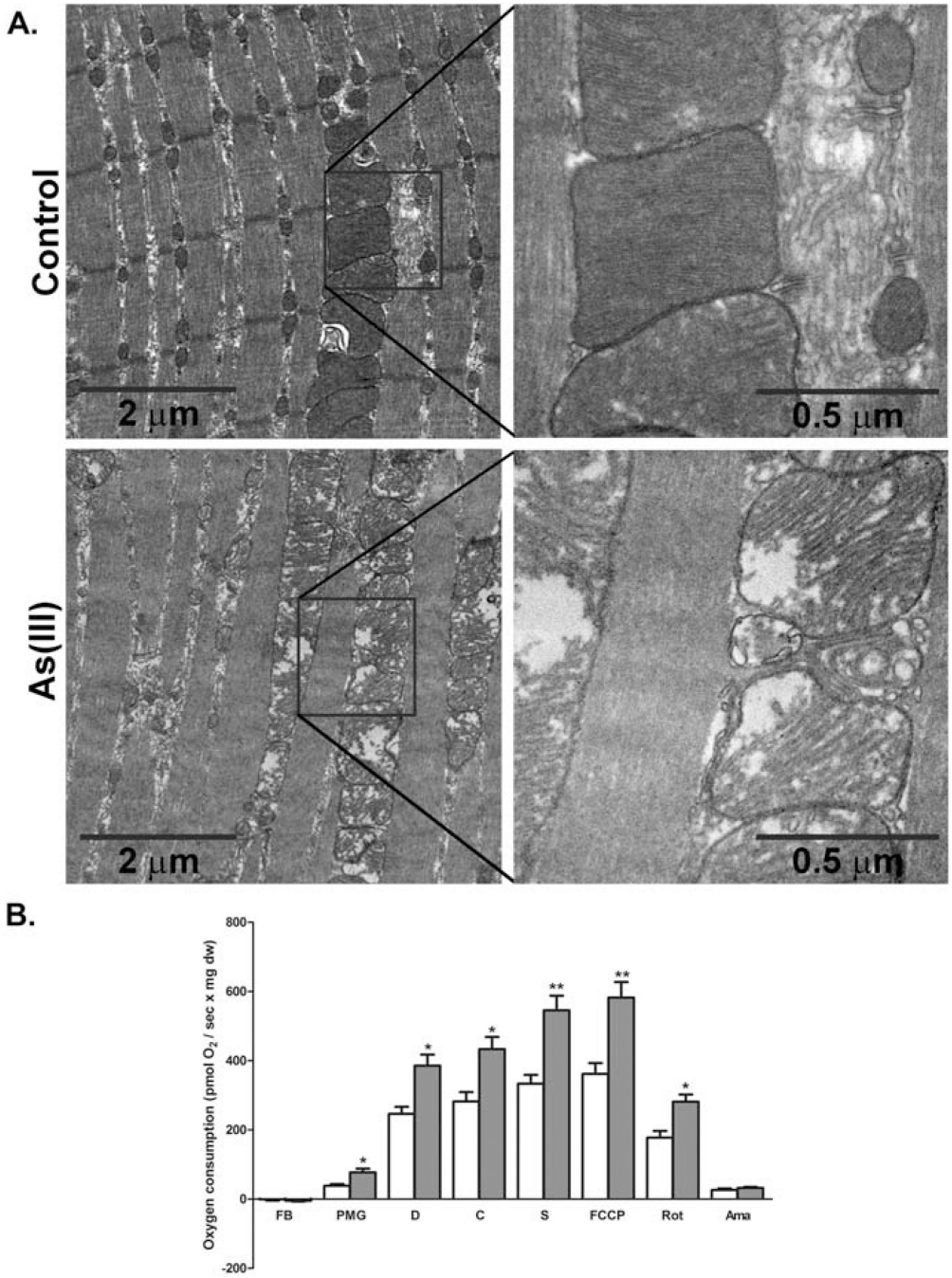

Figure 3.

Arsenic induces dysfuctional myofiber mitochondria and bioenergetics. **A**. Anterior tibialis muscles were fixed and processed for TEM as indicated in methods. The 10000× and 50,000× images demonstrate progressive ultrastuctural increases in myofiber width and mitochondrial size in mice exposed for 5 wk to 100 μg/L As(III), relative to 5 wk control mice. Images shown are representative of images from 6 mice/ group. **B**. Mitochondrial oxygen consumption was assessed using high-resolution respirometry in, permeablized myofibers, freshly isolated from control (open bar) and As(III)-exposed (grey bar) mice, as

described in methods. Additions to the oxygen consumption chamber were: **FB**: fiber bundles with no substrate, **PMG**: pyruvate, malate, glutamate, **D**: ADP, **C**: cytochrome C, **S**: succinate, **FCCP**: (uncoupled complex 1); **Rot**: rotenone (inhibited complex 1), Ama: antimycin A (inhibited complex 1 and 2). The data in the graph are mean ± SEM pmol/sec of oxygen consumption normalized to mg of tissue dry weight. Significance between consumption rates at each step for fibers from As(III) exposed mice relative to controls at $p<0.05$ is designated by * (t-test, n=5 mice in each group).

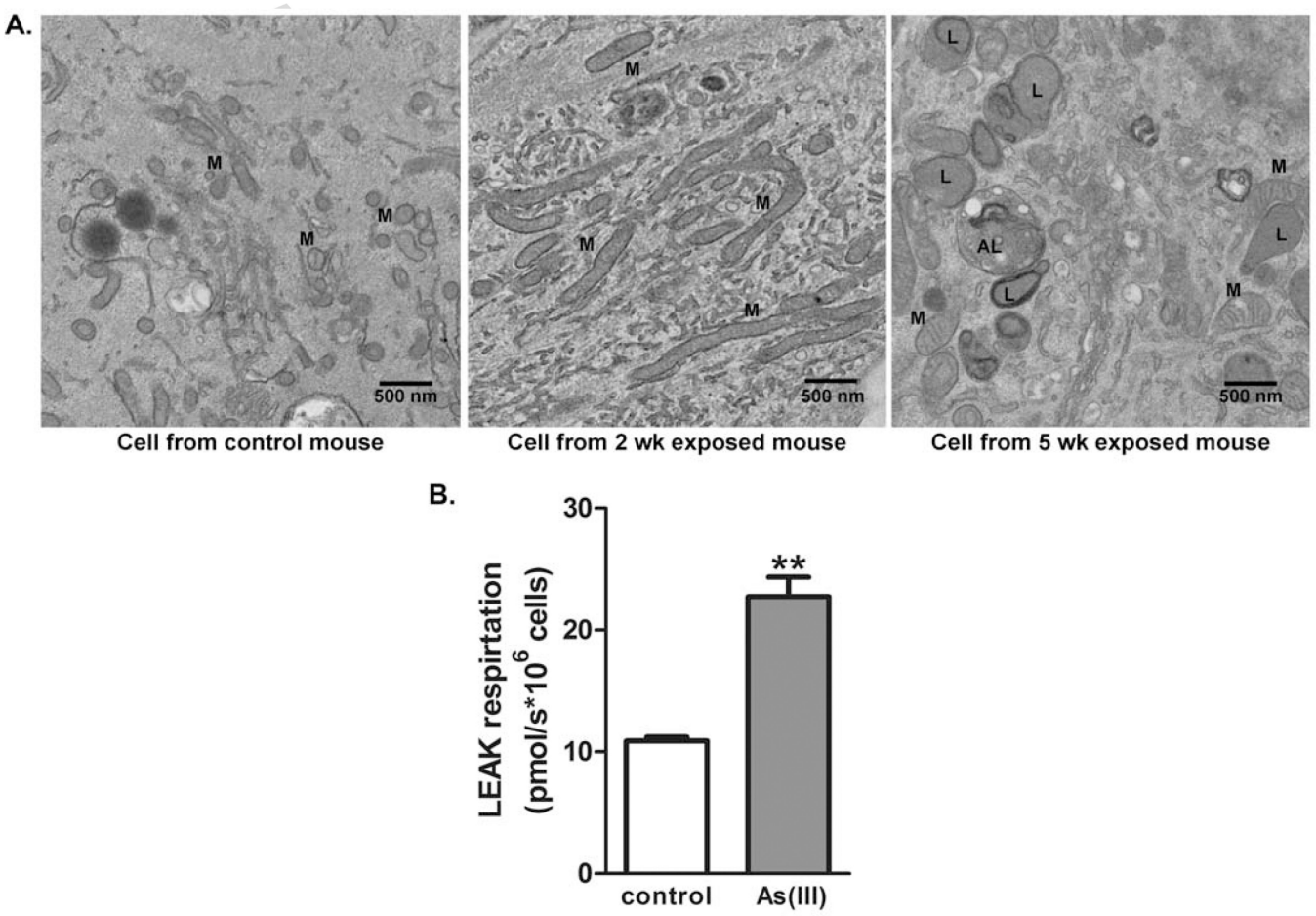

Figure 4.

Time dependent As(III)-induced dysfunctional muscle progenitor cell phenotype. Progenitor cells were isolated from hindlimb muscle of mice exposed to 0 or 100 ppb As(III) for 5 wk, as well as mice exposed to 100 μg/L As(III) for 2 wk. (A) Ultrastructural analysis by TEM imaging revealed that cells isolated from 2 and 5 wk As(III)-exposed mice retained the swollen and dysfunctional mitochondrial (M) phenotype. Cells isolated from 5 wk exposed mice indicated that the additional exposure induced a sustained increase of lyosomes (L) and autophagolysosomes (AL). The images are representative of multiple cells in replicate cultures of cells isolated from the different groups. (B). Mitochondrial-driven respiration was compared in progenitor cells isolated from control or 5 wk As(III)-exposed mice after expansion in culture without As(III), as described in methods. Nonphosphorylating LEAK respiration (electon flow coupled to proton pumping to compensate for proton leak) was measured in the presence of oligomycin. The data in the graph are mean ± SEM pmol of oxygen flow/sec per million cells. Significance between consumption rates at each step for fibers from As(III) exposed mice relative to controls of $p<0.002$ is designated by ** (t-test, n=4).

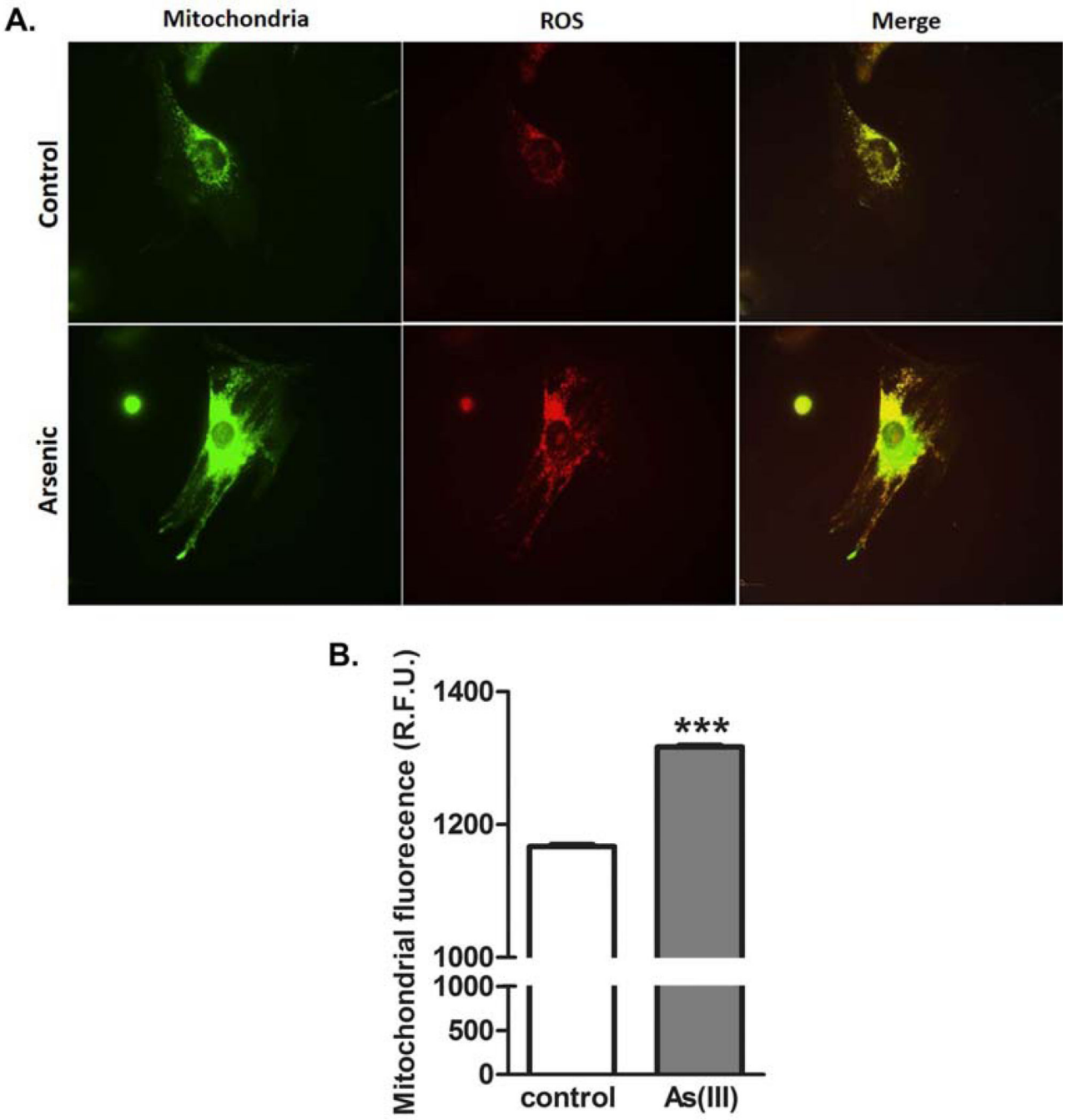

Figure 5.

As(III) induces a muscle progenitor cell phenotype with enhanced mitochondrial superoxide generation. Progenitor cells derived from control or As(III)-exposed mice were cultured without As(III) in chamber dishes for live cell confocal imaging of Mitosox™ Red dye oxydation. Cells were loaded with both Mitosox™ and Mito tracker® Green and followed over 30 minutes for change in respective fluoresence intensity. **A**. shows typical images of control cells and cells from As(III)-exposed mice. **B**. Fluorecent intensity of Mitosox™ relative to Mito tracker® was quantified and data are plotted as mean + SEM RFU for

2500–3000 cells in each culture. The data are repesentive of three replicate cell isolations and *** designates significant difference at $p<0.001$.

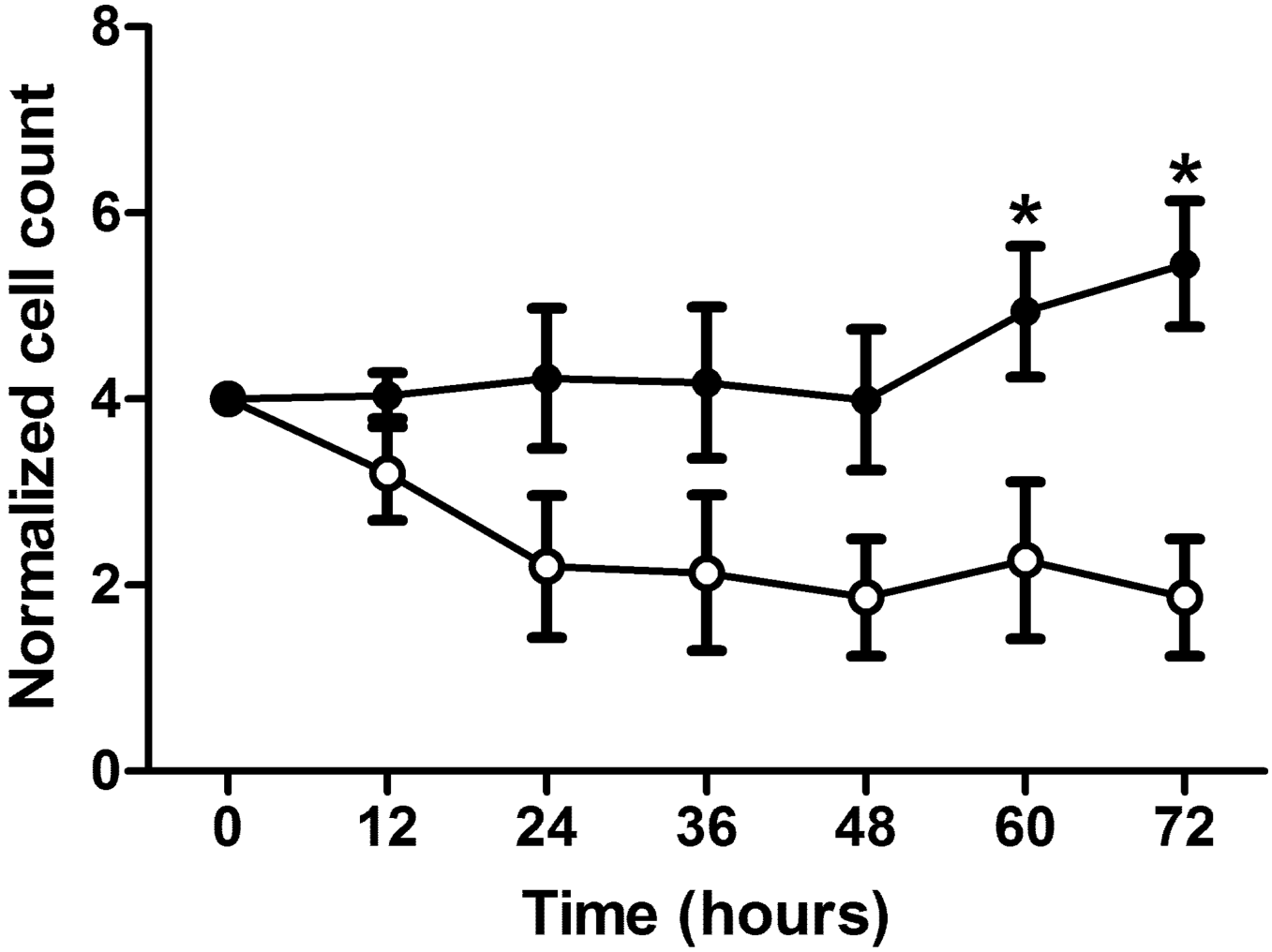

Figure 6.

As(III) induces a muscle progenitor cell phenotype that resists oxidant stress. Progenitor cells isolated from control or 5 wk As(III)-exposed mice were compared for cell number over 72 h following exposure to a toxic oxidative stress from 200μM H_2O_2. Cells from both groups were exposed to H_2O_2 at time=0 and cellular numbers were analyzed using Live Automated Cell Imaging. The data are normalized to the number of cells per 10× microscopic field with the same nine locations imaged at each time point in the respective cultures. * designates difference $p<0.05$ from respective control at the designated time point.

Table I

Arsenic and arsenic metabolite levels in muscle tissues. Data are the amount (ng) of arsenical per gram of muscle tissue as determined by hydride generation, HPLC separation and ICP-MS analysis (n=5 mice/group).

Treatment	Arsenic and Metabolites		
	iAs	monomethyarsenic	dimethylarsenic
Control	1.03 ± 0.80	0.62 ± 0.68	2.29 ± 0.79
Arsenic-exposed	0.94 ± 0.29	0.18 ± 0.07	1.61 ± 1.59

Table II

Arsenic effects on muscle and muscle contractile function. Data are presented as mean ± SEM and statistical differences were determined by standard t-tests (significance is indicated by bolded p-values)

Measurement	control	As(III)	p value
Mice (n)	6	5	
Muscle weight (mg)	49.2 ± 5.2	48.0 ± 4.3	p=0.35
Muscle length (mm)	11.6 ± 0.3	11.6 ± 0.2	p=0.34
Cross-sectional area (mm^2)	4.0 ± 0.3	3.9 ± 0.4	p=0.38
Maximum twitch torque (MilliNm)	0.7 ± 0.2	0.6 ± 0.1	p=0.39
Maximum tetanic torque, 120 Hz (MilliNm)	1.7 ± 0.2	1.9 ± 0.4	p=0.21
Specific twitch force ($MilliN/mm^2$)	5.4 ± 0.9	5.3 ± 0.9	p=0.42
Specific tetanic force, 120 Hz ($MilliN/ mm^2$)	14.0 ± 1.0	15.9 ± 2.3	p=0.055
Frequency for maximum specific tetanic force (Hz)	76.7 ± 9.2	108.0 ± 8.0	**p=0.03**
Time to peak twitch (s)	0.4 ± 0.1	0.3 ± 0.1	p=0.10
Half relaxation time (s)	0.003 ± 0.005	0.001 ± 0.001	p=0.18

Table III

Arsenic-induced muscle gene transcripts. Data are the amount of product relative amplified standards and normalized to housekeeping gene RPL41.

Gene	fg/ml of PCR product	
	Control	5 weeks Arsenic
Mitofusin2	2.5 ± 0.6	5.8 ± 1.1**
OPA1	0.7 ± 0.1	1.3 ± 0.2*
OMA 1	5.8 ± 0.4	10.0 ± 2.0**

* $p<0.05$;

** $p<0.01$. n=8 mice/group.